Journal of Colloid and Interface Science 700 (2025) 138513

Contents lists available at ScienceDirect

Journal of Colloid And Interface Science

journal homepage: www.elsevier.com/locate/jcis

The single-particle dynamics of square platelets on an inner spherical surface

Yue Shi [a,b,c,1], Fuzhou Liu [d,e,1], Yanran Li [a,b,c], Jianan Zhu [a], Mingcheng Yang [d,e,f,*], Kun Zhao [g,h,**], Yiwu Zong [a,b,c,***]

[a] School of Synthetic Biology and Biomanufacturing, Tianjin University, Tianjin 300072, China
[b] State Key Laboratory of Synthetic Biology and Frontiers Science Center for Synthetic Biology, Tianjin University, Tianjin 300072, China
[c] Frontiers Research Institute for Synthetic Biology, Tianjin University, Tianjin 300072, China
[d] Beijing National Laboratory for Condensed Matter Physics and Laboratory of Soft Matter Physics, Institute of Physics, Chinese Academy of Sciences, Beijing 100190, China
[e] School of Physical Sciences, University of Chinese Academy of Sciences, Beijing 100049, China
[f] Songshan Lake Materials Laboratory, Dongguan, Guangdong 523808, China
[g] Institute of Fundamental and Frontier Sciences, University of Electronic Science and Technology of China, Chengdu, Sichuan 610054, China
[h] The Sichuan Provincial Key Laboratory for Human Disease Gene Study and The Institute of Laboratory Medicine, Sichuan Provincial People's Hospital, University of Electronic Science and Technology of China, Chengdu, Sichuan 610054, China

HIGHLIGHTS

- Brownian squares exhibit sub-diffusive behavior on spherical surfaces.
- Translational dynamics weaken with increasing surface curvature.
- Rotational diffusion remains constant regardless of curvature changes.
- Smoluchowski equation matches experimental trends, highlighting geometric effect.
- A new way to quantitatively assess MSAD on spherical surfaces.

GRAPHICAL ABSTRACT

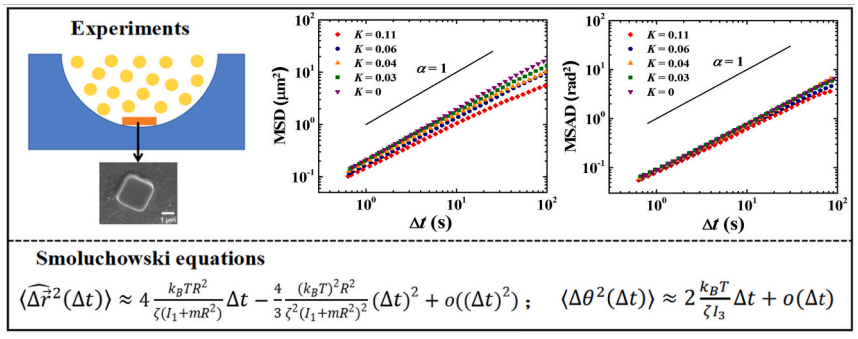

ARTICLE INFO

Keywords:
Colloidal squares
Curved surface
Curvature

ABSTRACT

Hypothesis: The diffusion of colloidal particles on curved surfaces is crucial for understanding mass transport in a wide range of biological and physical systems. To date, most experimental studies on colloid diffusion on curved surfaces have focused on the behavior of isotropic colloids diffusing on soft oil-water interfaces. However, there has been no experimental work reported on how anisotropic colloids diffuse on hard spherical surfaces.

* Corresponding author at: Beijing National Laboratory for Condensed Matter Physics and Laboratory of Soft Matter Physics, Institute of Physics, Chinese Academy of Sciences, Beijing 100190, China.
** Corresponding author at: Institute of Fundamental and Frontier Sciences, University of Electronic Science and Technology of China, Chengdu, Sichuan 610054, China.
*** Corresponding author at: School of Synthetic Biology and Biomanufacturing, Tianjin University, Tianjin 300072, China.
E-mail addresses: mcyang@iphy.ac.cn (M. Yang), kzhao@uestc.edu.cn (K. Zhao), yiwuzong@tju.edu.cn (Y. Zong).
[1] Yue Shi and Fuzhou Liu contribute equally to this work.

https://doi.org/10.1016/j.jcis.2025.138513
Received 25 March 2025; Received in revised form 7 July 2025; Accepted 21 July 2025
Available online 5 August 2025

Single-particle dynamics
Smoluchowski equations

Experiments: Herein, we report a first experimental study of the single-particle dynamics of micro-sized Brownian square platelets on solid spherical surfaces with four different curvatures. Utilizing video microscopy and particle-tracking techniques, we investigated both the translational and rotational motion of the square platelets. An analytical model based on Smoluchowski equations was developed to explain the observed diffusion behaviors.

Findings: The translational motion of the square platelets was found to be sub-diffusive at time scales comparable to their relaxation time, with the power-law exponent of the mean square displacement (MSD) decreasing as the curvature increased. In contrast, the rotational diffusion of the platelets exhibited minimal variation with changes in curvature. The developed analytical model based on Smoluchowski equations could explain the observations in both translational and rotational diffusion, highlighting the crucial role of surface geometry in determining the diffusion dynamics. This research provides new insights into the diffusion of anisotropic particles on hard spherical curved surfaces, which will pave the way for understanding mass transport problems on curved surfaces in various fields.

1. Introduction

The diffusion of colloids is a common phenomenon which is closely linked to life and many industrial processes [1–3]. Diffusion processes in cases of bulk 3-dimensional systems, near a 2-dimensional smooth plane or between two parallel planes have been widely studied and well understood [4–7]. In contrast, diffusion on curved surfaces remains relatively less explored. As colloidal diffusion on curved surfaces is related to many important mass transport processes [8–15] such as the diffusion of proteins inside cell membranes, or cell migrate on curved substrate [16] or under tubular confinement [17], a better understanding of how colloids diffuse on a curved surface will be of great importance. A primary model of curved surfaces used in previous studies is oil-water interfaces [18–20]. For example, Zhong et al. measured the trajectories of nano-sized polystyrene particles diffusing on highly curved water-silicone oil interface, and found that the diffusion of colloids slowed down as the curvature of oil droplet increased [18]. To date, the majority of studies on colloidal diffusion on curved surfaces have focused on soft oil-water interfaces, with relatively little attention given to diffusion on solid curved surfaces. However, diffusion on solid surfaces is equally important. The laws derived from soft interfaces cannot be directly applied to hard surfaces, as factors such as droplet deformation [18], oil viscosity [19,21,22], and recirculation effects [21], which influence diffusion on liquid-liquid interfaces, are absent on liquid-solid interfaces. Therefore, it is essential to investigate colloid diffusion on hard curved surfaces.

Anisotropic particles are widely distributed in nature, and have been applied in a large range of fields [23–25]. Understanding their diffusion processes especially their diffusion on curved surfaces is helpful to settle some important mass transport problems, such as the transport, accumulation, and bio-distribution of anisotropic drugs at the vascular level [26]. Compared to isotropic colloids, the dynamics of anisotropic ones is more complex due to the discernable rotational motion resulted from rotational symmetry breaking in their shapes [27–31]. Our previous experimental work discovered the effect of hard cylindrical curvature together with depletion attractions on translational and rotational motion of colloidal square platelets [32]. However, for how anisotropic colloids diffuse on another type of simple curved surface with nonzero Gaussian curvature - spherical surface, to the best of our knowledge, there is no experimental study reported yet. Herein, using video particle tracking techniques, we experimentally investigated the single-particle dynamics of Brownian square platelets on inner spherical surfaces with different curvatures in the presence of depletion agents, which was used to keep the square close to the substrate spherical surface with the normal direction of square's flat surfaces being parallel to the radial direction through depletion attractions between the square and the substrate spherical surface. Both translational and rotational diffusions of square platelets were investigated. By varying the radius of spherical surfaces, the effects of curvature on square diffusion were studied. An analytic model based on Smoluchowski equations have been developed and compared with our experimental measurements. The findings of this study highlight the significant role that substrate surface geometry plays in shaping the dynamics of anisotropic colloids, which may provide valuable insights and solutions for addressing a wide range of mass transport challenges.

2. Experimental part

2.1. Preparation of a sample cell containing spherical substrate surfaces

The process to fabricate a Polydimethylsiloxane (PDMS)-based sample cell containing spherical substrate surfaces is illustrated in Fig. 1a. First, cylindrical posts with different radii (between 5 μm and 25 μm) and the same height of 10 μm were deposited on a silicon wafer with positive photoresist EPG 590 (Everlight Chemical), as detailed in the Protocol in Supporting Information and Table S1 and Fig. S1. Then, the wafer was placed onto a hot plate (180 °C ~ 200 °C) for 3 min ~ 5 min to melt the cylindrical posts. After the wafer was cooled down to room temperature, spherical caps with different curvatures on the wafer were obtained, and the curvature of these caps were measured using the scanning electron microscope (SEM) images showing the side view of these caps (see one example in Fig. 1c). Next, we placed the wafer on the bottom of a small petri dish with the patterned side facing upwards, poured liquid PDMS (Dow Corning Sylgard 184 silicone elastomer kit, the ratio of pre-polymer to cross-linking agent is 10:1) into the petri dish, and let it cured in an oven at 80 °C for 20 min. After that, the crosslinked PDMS was peeled off, and bonded to a glass slide by oxygen plasma treatment for 45 s at 136 w. Then, a sample cell containing many spherical substrate surfaces was obtained. To observe the diffusion of colloids on spherical substrate surfaces, a volume of colloidal suspension was injected into the sample cell.

2.2. Colloidal suspensions

Square platelets with average edge length $L = 2.3 \pm 0.1$ μm and thickness of 1.2 ± 0.1 μm (a typical SEM image is shown in Fig. 1d) were made from SU-8 polymers (KAYAKU Advanced Materials) using photolithography in the same way as in our previous work [33]. To keep the square diffuses in close proximity to the inner spherical surface with the normal direction of square's flat surfaces being parallel to the radial direction, polystyrene particles with a diameter of 40 nm (by Thermo Fisher Scientific, Sulfate latex, 8 % w/v) was added into the system as depletion agents (the final concentration is 4 % w/v).

2.3. Sample preparation for the control experiment - colloids diffusing on a planar surface

First, the rectangular glass tube (VitroCom, 0.1 mm × 2 mm) was affixed to a glass slide using photosensitive adhesive (Norland NOA81). Subsequently, colloidal suspensions were introduced into the tube.

Finally, the tube was sealed with the same photosensitive adhesive (Norland NOA81).

2.4. Data collection and image analysis

Samples were observed with an inverted optical microscope (Leica DMi8) using a long working distance 63× objective (numerical aperture NA = 0.7). 10,000 images were taken by a sCMOS camera (ANDOR) at ~10 frames per second for each sample, which were then processed to extract centers and vertexes of squares for further analysis using user-written Interactive Data Language routines. As each taken image is in fact a projection of the observed object on a 2D flat plane, a coordinate transformation was performed to convert the extracted 2D coordinates of centers and vertexes of squares in each image back to the corresponding coordinates of squares on spherical surfaces in 3D space (see details in Supporting Information and Fig. S2-S3).

3. Results

We first studied the translational diffusion of squares on spherical substrate surfaces. The translational mean square displacement (MSD) is calculated as $\left\langle \widehat{\Delta \vec{r}}^{\,2}(\Delta t) \right\rangle = \left\langle |\vec{r}_i(t_1) \widehat{-} \vec{r}_i(t_0)|^2 \right\rangle$, where $\vec{r}_i(t_1)$ is the position vector of particle i (located on the curved surface) at time t_1, $\vec{r}_i(t_0)$ is the position vector of particle i at time t_0, Δt is time interval, and $|\vec{r}_i(t_1) \widehat{-} \vec{r}_i(t_0)| = \iota R$, represents the corresponding arc length of $\vec{r}_i(t_1) - \vec{r}_i(t_0)$ on the spherical surface, where ι is the central angle of the sphere between the center positions of the square at time t_0 and time t_1, R is the radius of the spherical surface, and $<\cdots>$ denotes ensemble average. As is shown in Fig. 2a, the MSD on the planar surface (curvature $K = 0$) is the largest among the tested conditions, and MSDs are reduced with K increases, indicating that the diffusion of squares on spherical surfaces will be more confined when K increases. Quantitatively, the

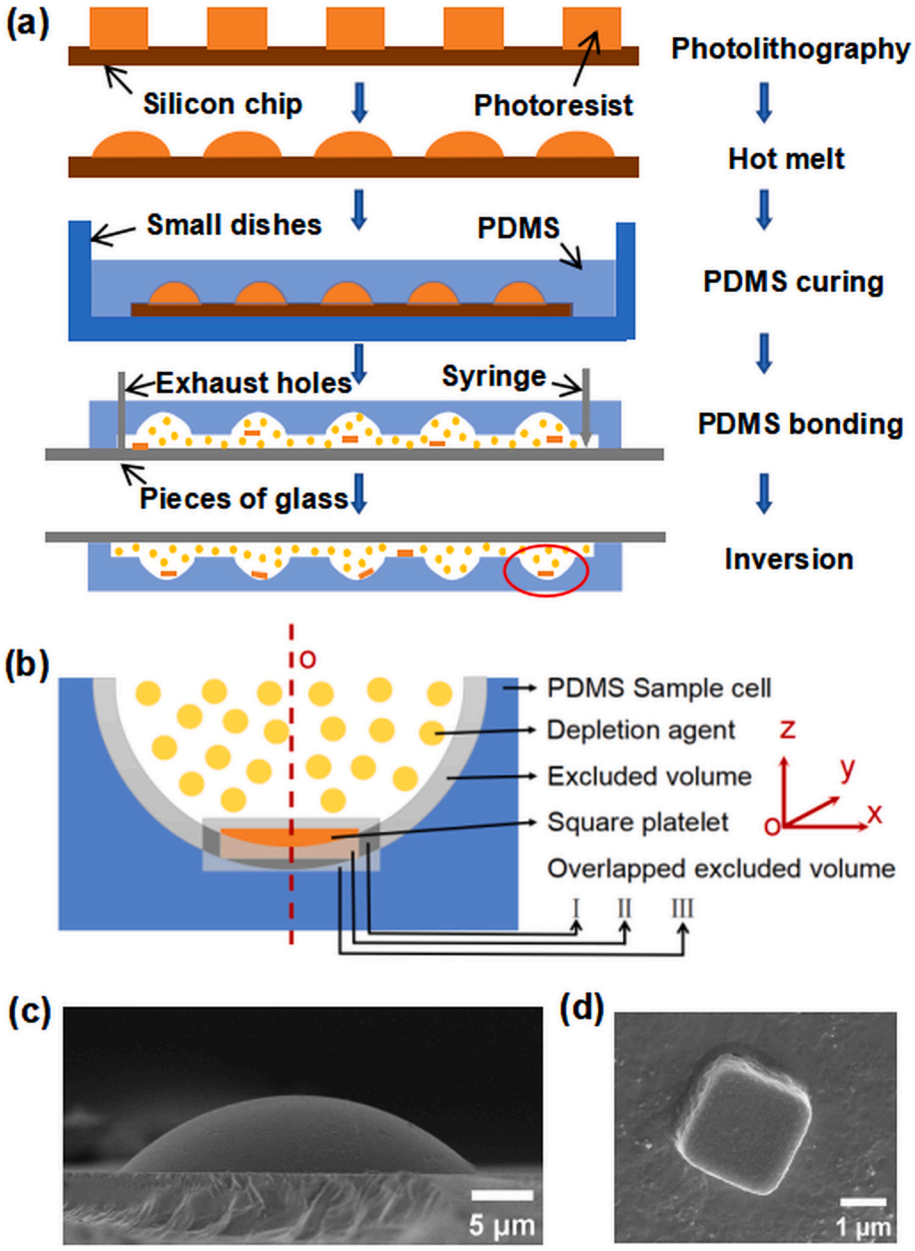

Fig. 1. (a) Fabrication of the sample cell with negative curved spherical caps on surface. (b) Schematic illustration to show the overlapped excluded volume between a square and the curved surface. (c) Scanning electron microscope image of a spherical cap on silicon wafer. Scale bar is 5 μm. (d) Scanning electron microscope image of a square platelet. Scale bar is 1 μm.

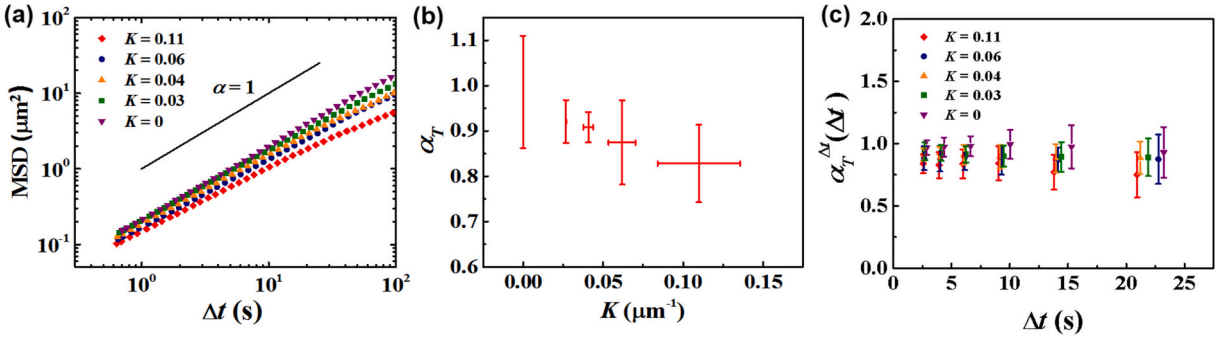

Fig. 2. (a) Mean square displacement (MSD) of a square on the inner surface of spherical caps with different curvature K. Red diamond: $K = 0.11\ \mu m^{-1}$; blue dot: $K = 0.06\ \mu m^{-1}$; yellow up triangle: $K = 0.04\ \mu m^{-1}$; green square: $K = 0.03\ \mu m^{-1}$; purple down triangle: planar surface. The black solid line corresponds to the slope equal to 1. (b) Translational diffusion index α_T of squares as a function of K. (c) Translational diffusion index $\alpha_T^{\Delta t}(\Delta t)$ of squares as a function of time interval Δt. Error bars represent the standard deviations of the corresponding data from 13 to 14 samples. (For interpretation of the references to colour in this figure legend, the reader is referred to the web version of this article.)

exponent α_T of the relationship MSD $\propto (\Delta t)^{\alpha_T}$ was calculated from a power law fitting of the data between 0.6 s and 20 s. Fig. 2b shows that α_T decreases from 0.99 ± 0.12 to 0.83 ± 0.09 as the curvature K changes from 0 to 0.11 μm^{-1}, suggesting that the translational diffusion of squares changes from a Brownian-type ($\alpha_T \sim 1$) to a sub-diffusive motion ($\alpha_T < 1$). Numerous theories and simulations [34–37] indicate that the particles on a curved surface would exhibit a normal diffusion at small but larger than the inertial time scale. Then, the expression $\alpha_T^{\Delta t}(\Delta t) = \frac{\partial \log \Delta r^2(\Delta t)}{\partial \log \Delta t}$ is employed to examine whether the MSD versus time interval curves shows a linear scaling at small time scales. As illustrated in Fig. 2c, even at very small time scales, the particles in our experiment still exhibit sub-diffusive behavior on the curved surface. For instance, at Δt is $\sim$ 9 s, the exponent $\alpha_T^{\Delta t}(\Delta t = 9s)$ decreases from 0.99 ± 0.12 on the planar surface to 0.90 ± 0.08, 0.90 ± 0.09, 0.87 ± 0.11, and 0.84 ± 0.14 on the curved surfaces with increasing curvature. For particles moving on the surface with the maximum spherical curvature ($K = 0.11$), the exponent continues to decrease as the time scale extends beyond 9 s. We would like to delve into this sub-diffusive behavior in conjunction with theoretical analysis in the following sections.

We then investigated the rotational diffusion of squares on spherical surfaces. For square diffusion on a planar surface, the angular displacement could be easily obtained by subtractions of square orientations. However, such simple calculation is not appropriate for diffusion on spherical surfaces, as the rotation of a square is referred to the axis that is perpendicular to the square flat surfaces and the orientation of this axis is changing when the square diffuses on spherical surfaces. To calculate the angular displacement of a square on a spherical surface,

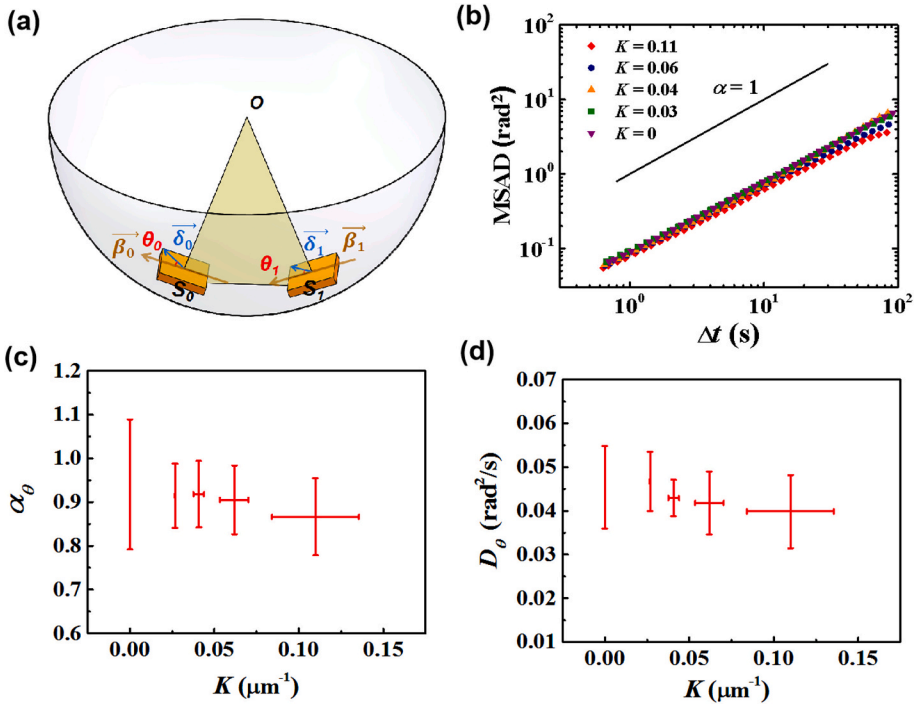

Fig. 3. (a) Schematic diagram showing the calculation of the angular displacement during a time interval t_1- t_0. (b) The mean square angular displacement (MSAD) of a square on the inner surface of spherical caps with different curvature. Red diamond: $K = 0.11\ \mu m^{-1}$; blue dot: $K = 0.06\ \mu m^{-1}$; yellow up triangle: $K = 0.04\ \mu m^{-1}$; green square: $K = 0.03\ \mu m^{-1}$; purple down triangle: planar surface. The black solid line corresponds to the slope equal to 1. (c) Rotational diffusion index α_θ and (d) rotational diffusion coefficient D_θ of squares as a function of K. D_θ is derived through a linear fit of the MSAD versus Δt curve, in conjunction with the relationship $\text{MSAD} = 2D_\theta \Delta t$. Error bars represent the standard deviations of the corresponding data from 13 to 14 samples. (For interpretation of the references to colour in this figure legend, the reader is referred to the web version of this article.)

we performed the following. Considering a square, at time t_0, its center is located at S_0 and has an orientational vector $\overrightarrow{\delta_0}$ pointing from S_0 to one of its corners, while at time t_1, it moves to S_1 and $\overrightarrow{\delta_0}$ becomes $\overrightarrow{\delta_1}$ (pointing from S_1 to the same corner as in $\overrightarrow{\delta_0}$) (Fig. 3). The plane of OS_0S_1 and the square flat surface will have an intersecting line, which is denoted as $\overrightarrow{\beta_0}$ for t_0, and $\overrightarrow{\beta_1}$ for t_1. We define the angle between $\overrightarrow{\delta_0}$ and $\overrightarrow{\beta_0}$ as θ_0, and similarly the angle between $\overrightarrow{\delta_1}$ and $\overrightarrow{\beta_1}$ as θ_1, then the angular displacement for the square diffusion on the spherical surface during the time interval $\Delta t = t_1 - t_0$, can be calculated as $\Delta\theta_i(\Delta t) = \theta_1 - \theta_0$, as illustrated in Fig. 3a. The $\Delta\theta_i(\Delta t)$ is clearly different from the angle between $\overrightarrow{\delta_0}$ and $\overrightarrow{\delta_1}$, which would the angle displacement if the square diffuses on a planar surface. For example, if the square moves from S_0 to S_1 without rotation around the square axis that is perpendicular to the square flat surface, for simplicity, we can also let $\overrightarrow{\delta_0}$ be parallel to $\overrightarrow{\beta_0}$, then $\theta_0 = 0$ and $\theta_1 = 0$, So $\Delta\theta_i(\Delta t) = 0$. However, $\overrightarrow{\delta_1} - \overrightarrow{\delta_0}$ is none zero (as $\overrightarrow{\delta_0}$ points upward whereas $\overrightarrow{\delta_1}$ points downward (Fig. S4). Using the aforementioned method, the mean square angular displacement (MSAD) was calculated as $\langle \Delta\theta^2(\Delta t) \rangle = \left\langle (\Delta\theta_i(\Delta t))^2 \right\rangle$, where <⋯> denotes ensemble average. The results are shown in Fig. 3b. Compared with MSD, there seems no conclusive trend in MSAD when K increases. By fitting the MSADs using a power law function MSAD $\propto (\Delta t)^{\alpha_\theta}$, the exponent α_θ of each MSAD curve on spherical surfaces was obtained. For the tested range of K, α_θ fluctuates between 0.91 ± 0.07 and 0.87 ± 0.09 (Fig. 3c), which is also close to the α_θ of the planar surface (0.92 ± 0.07), suggesting that the rotational diffusion of squares is not affected by the substrate surface curvature and is essentially a Brownian-type motion. The slight deviation of the averaged α_θ from 1 is likely due to the non-perfect conditions of fabricated spherical surfaces and colloids such as the roughness of substrate surfaces and square platelets. Correspondingly, the rotational diffusion coefficient D_θ measured based on MSAD curves also remains roughly constant when K changes (Fig. 3d).

To further understand the experimental observations, we first checked the role of depletion attractions in the diffusion behavior of squares. As the depletion agents were added into the system to keep squares diffusing close to the substrate surfaces, there is a face-to-face depletion attraction between a square and the substrate surface, which can be calculated to the first order by

$$U_{ff} = -V_e \times \Pi \quad (1)$$

where V_e is the overlapped excluded volume, Π is the osmotic pressure of depletion agents. Using an ideal gas approximation, Π is obtained by $\Pi = n_s k_B T$, where n_s is the number density of depletion agents and is calculated by $n_s = \varphi_s / (\pi d_s^3/6)$, with φ_s and d_s being the volume fraction and diameter of the spherical depletion agents, respectively. In this study, Π (or φ_s and d_s) keeps constant, so U_{ff} mainly changes with V_e, as V_e will change with the substrate surface curvature. For practical purposes, the calculation of V_e can be decomposed into three parts: The overlapped region between the excluded volume of the square and the excluded volume of the substrate (overlapped excluded volume I in Fig. 1b); The overlapped region between the square itself and the excluded volume of the substrate (overlapped excluded volume II in Fig. 1b); The overlapped region between the excluded volume of the square and the substrate itself (overlapped excluded volume III in Fig. 1b). These three parts can be numerically measured by constructing a 3D model where a square platelet falls to the bottom and sits stably on the spherical surface of a substrate with the normal axis of square flat surface along the radial direction of the spherical surface (illustrated in Fig. 1b), using SolidWorks software (see details in Supporting Information, Fig. S5 and Table S2). Thus, V_e and corresponding U_{ff} can be obtained for different spherical surfaces as substrates. The results are shown in Fig. 4., where U_{ff} was normalized by the magnitude of U_{ff}^{plane} for the case of planar substrate surface. We can see that the magnitude of

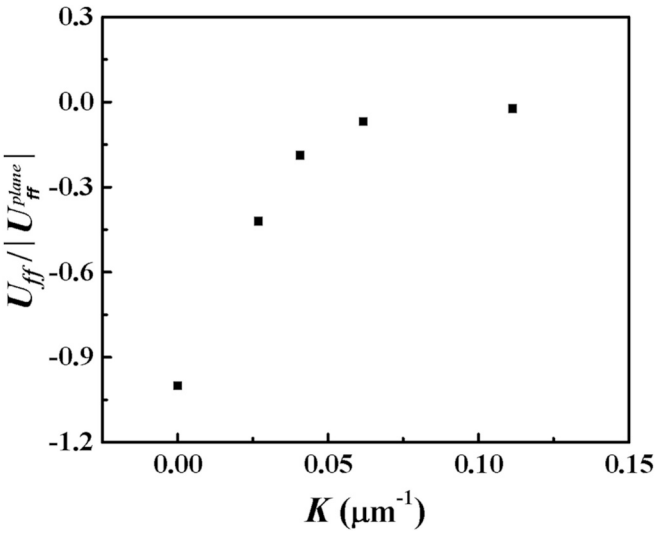

Fig. 4. The calculated face to face depletion attraction energy (U_{ff}) of a square on spherical surfaces normalized by the absolute depletion attraction energies on a flat surface ($|U_{ff}^{plane}|$), as a function of the curvature in the presence of 4 % (w/v) PS spheres with a diameter of 40 nm.

depletion attraction energy decreases as the curvature increases. From the lubrication theory [38,39], the drag coefficient of particles will decrease when they are further to the boundary surface (i.e., less affected by the boundary surface). Then, when the depletion attraction decreases as K increases, the square will be away from the substrate surface, and thus experience less drag imposed by the substrate surface, which should result in an enhancement in both translational and rotational dynamics as K increases. However, this contradicts to the experimental observations in Fig. 2c that translational diffusion declined on highly curved surfaces, suggesting that the depletion attraction is not the primary cause for the observed diffusion behavior on spherical surfaces. It is worth noting that in our experiment, the calculated depletion attraction between the square particles and the curved surfaces based on V_e ranges from 6.0 k_BT to 110.6 k_BT. Moreover, our microscopy videos show no significant detachment of the vertices of the squares from the surface. Thus, we conclude that the depletion attraction is sufficiently strong to enable the particles to diffuse along a spherical surface concentric with the substrate. This further supports the validity of our analytical methods for calculating the MSD and MSAD.

Once the particles diffuse away from the central valley position, gravity begins to influence their dynamics. Specifically, the larger the curvature of the spherical surface, the greater the tangential component of the gravitational force acting on the particles as they move along the surface of the sphere over the same distance. This enhanced tangential gravitational force exerts a stronger inhibitory effect on the translational motion of the particles. Consequently, in our experiments, gravity contributes to the observed decline in the exponent $\alpha_T^{\Delta t}(\Delta t)$ at short time scales for particles on the surface with the maximum curvature ($K = 0.11$ μm^{-1}). At long time scales, gravity can restrict the translational motion of particles on spherical curved surfaces. To investigate the impact of gravity on particle dynamics, we calculated the gravitational height (h_g) of the square particles (defined by $\Delta\rho V g h_g = k_B T$) and its corresponding arc length $\hat{r_g}$ for each spherical curved surface (see details in Supporting Information). Here, $\hat{r_g}$ represents the position along the surface, away from the central valley position, that is reached due to the thermal energy overcoming the particle's gravitational potential. To estimate the time scale t_g at which gravity starts to significantly suppress translational motion, we calculate t_g using the formula $t_g = \hat{r_g}^2 / D_T^{plane}$, where D_T^{plane} is the diffusion coefficient of the square platelets diffusing on a planar surface, as obtained from experimental measurements. The

results are summarized in Table 1. As shown in Table 1, all values of t_g exceed 100 s. This indicates that within our experimental time window of 100 s, gravity does not significantly restrict the translational motion of the particles, and thus does not lead to an MSD plateau.

Then, we turned to develop an analytical model for colloidal diffusion on spherical surfaces based on Smoluchowski equation. Following the work of Manca et al. [40], the Smoluchowski equation describing the motion of a Brownian particle on a surface S can be expressed as

$$\frac{\partial P}{\partial t} = \frac{k_B T}{\zeta}\Delta_g P \tag{2}$$

Here, *P is the probability density of the particle configuration*, k_B is the Boltzmann constant, T is the temperature, ζ is the friction coefficient per unit mass, $\frac{k_B T}{\zeta}$ is the product of translational diffusion coefficient and mass, and $g = \left[g_{ij}\right]$ represents the kinetic energy metric tensor, defined by$E_k = \frac{1}{2} g_{ij}\frac{dq^i}{dt}\frac{dq^j}{dt}$, where E_k is the kinetic energy and (q^i) is a set of generalized coordinates of the configuration space. The kinetic metric tensor g encodes the surface's geometric shape, thus incorporating geometric effects into the diffusion equation through the associated Laplacian operator Δ_g.

The kinetic energy of a thin small square platelet of mass m moving on a sphere of radius R is (derivation is given in Appendix A)

$$E_k = \frac{1}{2}\dot{\phi}^2\left[\sin^2\vartheta\left(I_1 + mR^2\right) + \cos^2\vartheta I_3\right] + \frac{1}{2}\dot{\vartheta}^2\left(I_1 + mR^2\right) + \frac{1}{2}\dot{\gamma}^2 I_3 + \dot{\phi}\,\dot{\gamma}\cos\vartheta I_3 \tag{3}$$

in which ϕ, ϑ denote the azimuth angle and the elevation angle of the center of mass of the platelet, respectively, and γ denotes the self-rotation angle of the platelet. I_1 represents the moment of inertia about the principal axes passing through the center of mass and parallel to one side of the square platelet, and I_3 denotes the moment of inertia about the axis passing through the center of mass and perpendicular to the plane of the square platelet. Hence the kinetic metric tensor in the coordinates $(\phi, \vartheta, \gamma)$ is

$$\left[g_{ij}\right] = \begin{bmatrix} \sin^2\vartheta\left(I_1 + mR^2\right) + \cos^2\vartheta I_3 & 0 & I_3\cos\vartheta \\ 0 & mR^2 + I_1 & 0 \\ I_3\cos\vartheta & 0 & I_3 \end{bmatrix} \tag{4}$$

The associated Laplacian operator is

$$\Delta_g = \frac{1}{\left(I_1 + mR^2\right)\sin^2\vartheta}\frac{\partial^2}{\partial\phi^2} + \frac{1}{I_1 + mR^2}\frac{\partial^2}{\partial\vartheta^2} + \frac{\cot\vartheta}{I_1 + mR^2}\frac{\partial}{\partial\vartheta} - 2\frac{\cos\vartheta}{\left(I_1 + mR^2\right)\sin^2\vartheta}\frac{\partial^2}{\partial\phi\partial\vartheta} + \frac{\left(I_1 + mR^2\right)\sin^2\vartheta + I_3\cos^2\vartheta}{I_3\left(I_1 + mR^2\right)\sin^2\vartheta}\frac{\partial^2}{\partial\gamma^2} \tag{5}$$

It can be shown that the solution of the Smoluchowski eq. (2) admits a small-time expansion [41]:

$$\langle f(t)\rangle_{x_0=y} = \sum_{k=0}^{\infty}\frac{t^k}{k!}\left\langle\left(\mathscr{D}\Delta_g\right)^k f\right\rangle_{x_0=y} = \sum_{k=0}^{\infty}\frac{t^k}{k!}\mathscr{D}^k\Delta_g^k f(y) \tag{6}$$

Here, $\langle f(t)\rangle_{x_0=y}$ represents the ensemble average of a function f depending on the position x of the system at time t, with the system starting from an initial position $x_0 = y$, $\mathscr{D} = \frac{k_B T}{\zeta}$, and Δ_g is the Laplacian operator.

For the square plate system considered in this study, the quantities of interest are the MSD ($\left\langle \widehat{\Delta\vec{r}}^{\,2}(\Delta t)\right\rangle$), the MSAD ($\langle\Delta\theta^2(\Delta t)\rangle$), and a direct calculation (details given in Appendix B) shows that the dependence of the MSD and MSAD on the curvature radius R of the spherical surface is

$$\left\langle \widehat{\Delta\vec{r}}^{\,2}(\Delta t)\right\rangle \approx 4\frac{k_B T R^2}{\zeta\left(I_1 + mR^2\right)}\Delta t - \frac{4}{3}\frac{(k_B T)^2 R^2}{\zeta^2\left(I_1 + mR^2\right)^2}(\Delta t)^2 + o\left((\Delta t)^2\right) \tag{7}$$

$$\langle\Delta\theta^2(\Delta t)\rangle \approx 2\frac{k_B T}{\zeta I_3}\Delta t + \frac{(k_B T)^2}{\zeta^2\left(I_1 + mR^2\right)^2}(\Delta t)^2 + o\left((\Delta t)^2\right) \tag{8}$$

In particular, the power series expansions presented in eqs. (7) and (8) can be regarded as specific instances of the mean-square geodesic displacement expansion formula given in literature [42], which is expressed as '$\left\langle[\delta s(t)]^2\right\rangle \approx 4Dt - \sum_{n=2} G_n[K_G(x_0)](Dt)^n$'.

For the MSD Eq. (7), the coefficient of the linear term is $4\frac{k_B T R^2}{\zeta\left(I_1+mR^2\right)} \sim 4.2 \times 10^{-13}$ m^2/s, while the one for the quadratic term, $-\frac{4}{3}\frac{(k_B T)^2 R^2}{\zeta^2\left(I_1+mR^2\right)^2}$, ranges from -3.1×10^{-16} to -1.1×10^{-17} m^2/s^2 in our experiments, which is approximately three orders of magnitude smaller than that of the linear term. By contrast, for the MSAD Eq. (8), the coefficient of the quadratic term, $\frac{(k_B T)^2}{\zeta^2\left(I_1+mR^2\right)^2}$, ranges from 5.8×10^{-9} to 4.9×10^{-6} rad^2/s^2, which is at least five orders of magnitude smaller than the linear coefficient $2\frac{k_B T}{\zeta I_3} = 0.24$ rad^2/s. Given that the experimental time scale can reach the order of 100 s, for MSD Eq. (7), the quadratic term is considerable, while for MSAD Eq. (8), the quadratic term is negligible. It is worth noting that the experimental time scale is comparable to the translational relaxation timescale (estimated with $L^2/D_T^{plane} \sim 140.8$ s), but is significantly shorter by an order of magnitude compared to the rotational relaxation timescale (estimated by $(2\pi)^2/D_\theta^{plane} \sim 44.5$ min, where D_θ^{plane} is the rotational diffusion coefficient of the square platelets diffusing on a planar surface, as obtained from experimental measurements). Thus, the experimental timescale is intermediate for translational motion and quite short for rotational motion in the context of Brownian dynamics. Based on the above considerations, for the MSD described by Eq. (7), we retain the quadratic term. In contrast, for the MSAD given by Eq. (8), the quadratic term is found to be negligible. This allows us to simplify Eq. (8) to Eq. (9).

$$\langle\Delta\theta^2(\Delta t)\rangle \approx 2\frac{k_B T}{\zeta I_3}\Delta t + o(\Delta t) \tag{9}$$

For the MSD, given that $I_1 = mL^2/12$ ($\sim 3.1 \times 10^{-27}$ kg/m^2), the term mR^2 (3.3×10^{-25}–9.7×10^{-24} kg/m^2) is significant in Eq. (7). Consequently, the coefficient of the linear term can be approximated to be $4\frac{k_B T}{\zeta m}$. Then, at short time scales, when the second quadratic term in Eq. (7) is negligible compared with the linear term, the power-law exponent of the MSD is predicted to be 1, and the diffusion coefficient nearly remains constant for different curvatures. At intermediate time scales, however, the quadratic term has contributions. Again, given $mR^2 >> I_1$, the quadratic term coefficient $-\frac{4}{3}\frac{(k_B T)^2 R^2}{\zeta^2\left(I_1+mR^2\right)^2} \propto -1/R^2$, then it decreases with increasing curvature, which will lead to the deviation of the power law exponent of MSD from 1 as the curvature increases, consistent with the experimental results (Fig. 2b). Specifically, the complex metric tensor of the system endows the $(\phi, \vartheta, \gamma)$ configuration space with a non-Euclidean geometric structure. This curvature-induced distortion manifests in the Laplacian (e.g., through the $\frac{\cot\vartheta}{I_1+mR^2}\frac{\partial}{\partial\vartheta}$ term in Eq. (5)), modifying the solution of the Smoluchowski equation. As a result, the probability density evolution no longer adheres to a standard Gaussian distribution with linearly increasing variance, ultimately leading to the observed deviation from linear MSD scaling at longer times. The gravitational force acting on the particles further exacerbates this deviation. For MSAD, the linear term in Eq. (9) predicts the power law exponent of

Table 1
The calculated h_g, $\hat{r_g}$ and t_g for spherical surfaces with different K.

K (μm^{-1})	h_g (μm)	$\hat{r_g}$ (μm)	t_g (s)
0.11	0.348	2.6	180
0.06	0.348	3.4	308
0.04	0.348	4.1	447
0.03	0.348	5.1	692

MSAD at short time scales is 1 and the rotational diffusion coefficient D_θ shall be independent of the curvature, which matches well with the experimental results (Fig. 3c and 3d).

The expression of Eq. (7) hints that if we define a dimensionless time $\tau = \mathscr{D}\Delta t/\left(I_1 + mR^2\right)$, the small-time power series expansion of MSD can be written as

$$\left\langle \widehat{\Delta \vec{r}}^{\,2}(\Delta t) \right\rangle = f(\tau) = a_0 + a_1\tau + a_2\tau^2 + \cdots \tag{10}$$

where $f(\tau)$ is a function of τ. This conjecture can be verified analytically. By solving the Smoluchowski equation Eq. (2), one can obtain the explicit expression of $f(\tau)$, as given by Eq. (C5) in Appendix C. This expression is, in principle, valid across all time scales.

The comparison between the experimental measurements of MSD and the theoretical predictions is shown in Fig. 5a. At early times, the experimental data and the theoretical predictions are in excellent agreement. However, as the value of τ exceeds 10^{-3}, the experimental curve shows a slower growth than theoretical prediction. This discrepancy may be attributed to the effect of gravity, which restricts the particles from exploring the full configuration space of the sphere, thereby leading to a slower long-time diffusion behavior. Another notable observation is that when the dimensionless time τ is taken as the x-axis, the MSD curves normalized by surface curvatures for each different substrate surface collapse onto a common one. This further supports the validity of the Smoluchowski theory.

On the other hand, calculating the full-time-scale MSAD formula theoretically is much more challenging than that of the MSD. Therefore, in comparing experimental MSAD data with theoretical predictions, we use the small-time expansion given by Eq. (8) as our theoretical benchmark. As shown in Fig. 5b, the experimental MSAD data align well with the theoretical prediction across the entire observation time scale. This close agreement indicates that the dynamics of MSAD exhibit a small-time free-diffusion characteristic throughout the entire observation time interval.

4. Conclusions

In this study, we have experimentally studied the single-particle diffusive behavior of Brownian square platelets on spherical surfaces with four curvatures ranging from 0.03 μm^{-1} to 0.11 μm^{-1}. For translational diffusion, the squares showed sub-diffusive behavior at short time scale (50 s, comparable to the relaxation time) on spherical surfaces. Moreover, the exponent of the mean square displacement (MSD) decreased as the curvature increased. In contrast, other research groups studying particle diffusion at oil-water interfaces have focused on the diffusion coefficient in the linear regime of MSD and have concluded that the diffusion coefficient of particles decreases as the size of the oil droplet becomes smaller [18,20]. Danov et al. have shown that the recirculation effect influences particle motion at liquid-liquid interfaces when the ratio of the droplet radius to the particle radius is relatively small [21]. However, the recirculation effect and the diffusion-induced droplet deformation discussed in other work [18] do not apply to solid surfaces. By applying the Smoluchowski equation to a spherical surface, we demonstrated that the derived model aligns remarkably well with the observed trend of decreasing translational diffusion index α_T as curvature K increases in our experiments. This consistency indicates that the geometric effect of the spherical surface plays a significant role in the colloidal translational dynamics. One of the reasons to have different particle dynamics on soft and hard interfaces may be due to the fact that when particles come into contact with a soft interface, deformation occurs at the point of contact. This deformation can significantly diminish the influence of local curvature, thereby reducing the impact of geometric effects on particle dynamics. However, to test this hypothesis, more future work is needed.

For rotational diffusion, we note that our work is the first experimental investigation of the rotational motion of colloids on spherical surfaces with varying curvatures since rotations of squares can be easily discerned. Moreover, considering that angular displacement on spherical surfaces cannot be directly obtained by subtracting square orientations, in this study we proposed a new way to quantitatively assess the angular displacement for anisotropic particles diffusing on spherical surfaces. The proposed new method can also be applied for evaluating rotational motion on curved surfaces in related studies. Unlike translational behavior, the measured rotational results revealed that rotational dynamics remained unchanged as curvature varied, which aligns with predictions from the Smoluchowski equation. The consistency observed between experiments and models in both translational and rotational motions underscores the significant impact of spherical surface geometry on colloidal diffusion.

The colloidal diffusion on curved surfaces is a complex process influenced by various factors, including the geometric properties of the surface, hydrodynamic interactions, gravity and depletion attractions in our system. Our previous work revealed that depletion attractions play a critical role in the diffusion of square platelets on cylindrical surfaces, particularly in their rotational motion [32]. Specifically, the fluctuation range of the orientational angle of squares is significantly reduced in cylinders with high curvature due to the orientation-dependent depletion attractions. In contrast, on spherical surfaces our numerical results demonstrate that the depletion attraction weakens as the curvature of the spherical surface increases. Thus, in this study it is not the depletion attraction but the geometry of the substrate surface that primarily hinders the translational diffusion of squares on highly curved surfaces, thus uncovering a crucial role that the substrate geometry plays in the diffusion of squares. Future work could investigate whether such effect of substrate geometry is particle-shape dependent or not by testing other

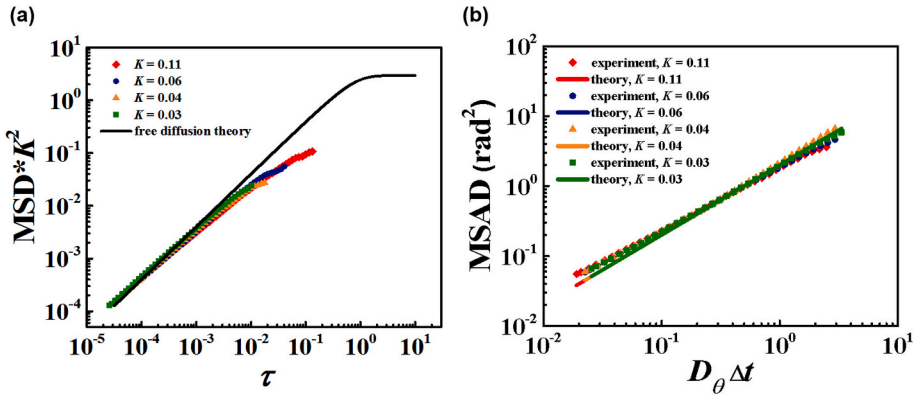

Fig. 5. Comparison of experimental measurements of mean squared displacement (MSD) (a) and mean square angular displacement (MSAD) (b) with theoretical predictions.

anisotropic particle shapes, such as triangular or pentagonal platelets, to further elucidate the interplay between particle shape and substrate surface geometry.

Our research offers new insights into the diffusion of anisotropic particles on hard spherical surfaces, providing valuable perspectives and potential solutions for a broad range of mass transport challenges. Additionally, the method for fabricating PDMS-based sample cells with spherical surfaces, as well as the approach developed in this study to measure mean squared angular displacement (MSAD) on spherical surfaces, are both practical and easily adaptable. These methods can be readily extended to investigate the diffusion of other anisotropic particles on curved surfaces, thereby enriching the work on the dynamics of anisotropic particles on hard spherical surfaces.

CRediT authorship contribution statement

Yue Shi: Writing – original draft, Methodology, Formal analysis, Data curation. **Fuzhou Liu:** Writing – original draft, Methodology, Formal analysis. **Yanran Li:** Writing – review & editing, Investigation, Formal analysis, Data curation. **Jianan Zhu:** Software, Methodology. **Mingcheng Yang:** Writing – review & editing, Supervision, Methodology, Formal analysis. **Kun Zhao:** Writing – review & editing, Validation, Supervision, Methodology, Funding acquisition, Formal analysis, Conceptualization. **Yiwu Zong:** Writing – review & editing, Writing – original draft, Validation, Supervision, Software, Methodology, Investigation, Formal analysis, Conceptualization.

Declaration of competing interest

The authors declare the following financial interests/personal relationships which may be considered as potential competing interests: Kun Zhao reports financial support was provided by National Natural Science Foundation of China. If there are other authors, they declare that they have no known competing financial interests or personal relationships that could have appeared to influence the work reported in this paper.

Acknowledgements

We thank the technical support provided by Space Application System of China Manned Space Program. This work is supported by the Space Application System of China Manned Space Program (TGTZYY00-WL-JY-000), and the National Natural Science Foundation of China (12374206).

Appendix A. Derivation of Eq. (3).

For a square platelet with side length a moving on a sphere of radius R, its center of mass lies on a sphere of radius $R' = \sqrt{R^2 - a^2}$. When a≪R, we can reasonably assume that $R' \approx$ R. The geometric orientation of the platelet can be described by three Euler angles [43] α, β, γ, in which α is the precession angle, β is the nutation angle, and γ is the self-rotation angle. The corresponding rotational matrix is

$$R(\alpha,\beta,\gamma) = \begin{bmatrix} \cos\gamma & \sin\gamma & 0 \\ -\sin\gamma & \cos\gamma & 0 \\ 0 & 0 & 1 \end{bmatrix} \bullet \begin{bmatrix} 1 & 0 & 0 \\ 0 & \cos\beta & \sin\beta \\ 0 & -\sin\beta & \cos\beta \end{bmatrix} \bullet \begin{bmatrix} \cos\alpha & \sin\alpha & 0 \\ -\sin\alpha & \cos\alpha & 0 \\ 0 & 0 & 1 \end{bmatrix} \tag{A1}$$

Let $\mathbf{e}_1$,$\mathbf{e}_2$,$\mathbf{e}_3$ be the principal axes of inertial of the platelet at a reference configuration(with $\mathbf{e}_3$ perpendicular to the platelet), then after an arbitrary rigid body motion specified by the Euler angles α, β, γ, the principal axes become $\mathbf{k}_i = R(\alpha,\beta,\gamma)\cdot\mathbf{e}_i$. In particular,

$$\mathbf{k}_3 = (\sin\alpha\sin\beta, -\cos\alpha\sin\beta, \cos\beta) \tag{A2}$$

For a square platelet moving on a sphere, the geometric constraint implies that $\mathbf{k}_3$ is perpendicular to the tangent plane of the sphere at the center of mass, whose normal vector can be described in spherical coordinates ϕ, ϑ by

$$\mathbf{n} = (\sin\vartheta\cos\phi, \sin\vartheta\sin\phi, \cos\vartheta) \tag{A3}$$

Identifying $\mathbf{k}_3$ with $\mathbf{n}$, we arrive at the relation

$$\begin{cases} \alpha = & \pi/2 + \phi \\ \beta = & \vartheta \end{cases} \tag{A4}$$

According to Euler's theorem, the rotation of a rigid body about a fixed point can always be represented as a rotation about a fixed axis. The angular velocity $\boldsymbol{\omega}$ is directed along this axis, and can be expressed as

$$\boldsymbol{\omega} = \omega_1\mathbf{k}_1 + \omega_2\mathbf{k}_2 + \omega_3\mathbf{k}_3 = [\,\mathbf{k}_1 \quad \mathbf{k}_2 \quad \mathbf{k}_3\,]\cdot\begin{bmatrix} \sin\beta\sin\gamma & \cos\gamma & 0 \\ \sin\beta\cos\gamma & -\sin\gamma & 0 \\ \cos\beta & 0 & 1 \end{bmatrix}\cdot\begin{bmatrix} \dot{\alpha} \\ \dot{\beta} \\ \dot{\gamma} \end{bmatrix} \tag{A5}$$

Substituting (A4) into (A5), one can find that the rotational kinetic energy of the rigid body is

$$E_{\text{rot}} = \frac{1}{2}\left(I_1\omega_1^2 + I_2\omega_2^2 + I_3\omega_3^2\right) = \frac{1}{2}\dot{\phi}^2\sin^2\vartheta I_1 + \frac{1}{2}\dot{\vartheta}^2 I_1 + \frac{1}{2}(\dot{\phi}\cos\vartheta + \dot{\gamma})^2 I_3 \tag{A6}$$

where I_i is the moment of inertia of the rigid body about the principal axis $\mathbf{e}_i$.The total kinetic energy of the system is the sum of rotational kinetic energy and translational kinetic energy of the center of mass:

$$\begin{aligned} E_{\text{tot}} = & \quad E_{\text{tran}} + E_{\text{rot}} = \frac{1}{2}mR^2\left(\dot{\vartheta}^2 + \sin^2\vartheta\dot{\phi}^2\right) + E_{\text{rot}} \\ = & \quad \frac{1}{2}\dot{\phi}^2\left[\sin^2\vartheta\left(I_1 + mR^2\right) + \cos^2\vartheta\, I_3\right] + \frac{1}{2}\dot{\vartheta}^2\left(I_1 + mR^2\right) + \frac{1}{2}(\dot{\phi}\cos\vartheta + \dot{\gamma})^2 I_3 \end{aligned} \tag{A7}$$

Appendix B. Derivation of Eqs. (7) and (8).

Eq. (5) provides the expression for the Laplacian operator, which is a linear combination of first-order partial differential operators and the squares of these operators. Let $f = (R\vartheta)^2$ be the sqaure displacement of a single platelet, a direct calculation yields

$$\Delta_g f = \frac{R^2}{I_1 + mR^2}(2 + 2\vartheta\cot\vartheta) \tag{B1}$$

At the initial position x_0, without loss of generality we can assume that $\vartheta = 0$, hence

$$\Delta_g f\big|_{x_0} = \frac{4R^2}{I_1 + mR^2} \tag{B2}$$

Similarly, let $h = (\Delta\theta)^2$ be the square angular displacement of a single platelet, from Fig. 3 one can observe that

$$\Delta\theta = \Delta\phi + \Delta\gamma \tag{B3}$$

Therefore

$$\Delta_g h = \frac{1}{I_1 + mR^2}\left(\frac{2}{\sin^2\vartheta} + 2\cot^2\vartheta - 4\frac{\cos\vartheta}{\sin^2\vartheta}\right) + \frac{2}{I_3} \tag{B4}$$

Hence

$$\Delta_g h\big|_{x_0} = \frac{2}{I_3} \tag{B5}$$

On the other hand, apply Δ_g to f twice gives

$$\Delta_g^2 f = \frac{R^2}{I_1 + mR^2}\Delta_g(2 + 2\vartheta\cot\vartheta) = \frac{2R^2}{(I_1 + mR^2)^2}\left(\cot^2\vartheta - \frac{2}{\sin^2\vartheta} + \frac{\vartheta\cot\vartheta}{\sin^2\vartheta}\right) \tag{B6}$$

Hence

$$\Delta_g^2 f\big|_{x_0} = -\frac{8}{3}\frac{R^2}{(I_1 + mR^2)^2} \tag{B7}$$

Apply Δ_g twice to h gives

$$\Delta_g^2 h = 2\frac{\sec^4(\vartheta/2)}{(I_1 + mR^2)^2} \tag{B8}$$

Hence

$$\Delta_g^2 h\big|_{x_0} = \frac{2}{(I_1 + mR^2)^2} \tag{B9}$$

Eqs. (7) and (8) can be readily obtained by substituting (B2), (B5), (B7) and (B9) into eq. (6).

Appendix C. Derivation of the Theatrical Prediction of Eq. (10).

The solution of the Smoluchowski eq. (2) can be expressed as

$$P(\theta, \phi, \gamma, t) = \sum_{n,k,\ell} e^{\lambda_{n,k,\ell} Dt}\langle u_{n,k,\ell}|P_0\rangle u_{n,k,\ell}(\theta, \phi, \gamma) \tag{C1}$$

Here n ranges in all non-negative integers, and k and ℓ ranges in all integers, $\langle f|h\rangle$ is the inner product between complex-valued functions defined by

$$\langle f|h\rangle = \int_0^{2\pi} d\phi \int_0^{2\pi} d\gamma \int_0^{\pi} \sqrt{G}\, d\theta\, f^*(\theta, \phi, \gamma) h(\theta, \phi, \gamma) \tag{C2}$$

In Eq.(C2), $G = I_3(I_1 + mR^2)^2\sin^2\theta$ is the determinant of the metric tensor g. The eigenfunctions $(u_{n,k,\ell})$ of the Laplacian operator Δ_g form a complete orthonormal basis of the Hilbert function space, and are given by

$$u_{n,k,\ell}(\theta, \phi, \gamma) = A_{n,k,\ell} e^{ik\gamma} e^{i\ell\phi}\sin^{|k-\ell|}(\theta/2)\cos^{|k+\ell|}(\theta/2) P_n^{(|k-\ell|,|k+\ell|)}(\theta) \tag{C3}$$

in which $A_{n,k,\ell}$ is the normalization factor, and $P_n^{(\alpha,\beta)}$ is the Jacobi polynomial [44]. The associated eigenvalue is

$$\lambda_{n,k,\ell} = -\frac{1}{I_1 + mR^2}\left[n(n+1) + \max\{|k|, |\ell|\}(\max\{|k|, |\ell|\} + 2n + 1) + \frac{I_1 + mR^2 - I_3}{I_3}k^2\right] \tag{C4}$$

Averaging the function θ^2 with respect to the right-hand side of Eq.(C1) leads to

$$\langle\theta^2\rangle = \sum_{n=0}^{\infty} \frac{2n+1}{2} g_{\theta^2}(n) e^{-n(n+1)\mathscr{D}\Delta t/(I_1 + mR^2)} \tag{C5}$$

in which $g_{\theta^2}(n) = \int_0^{\pi} \mathrm{d}\theta P_n^{(0,0)}(\cos\theta)\theta^2 \sin\theta$ is a geometric factor. The eq. (C5) is consistent with the eq. (D6) in literature [45], which describes the MSAD of a Brownian particle moving on a sphere. Now define the dimensionless time $\tau = \mathscr{D}\Delta t/\left(I_1 + mR^2\right)$ and the desired expression of $\left\langle \widehat{\Delta \vec{r}}^{\,2}(\Delta t) \right\rangle = f(\tau)$ follows.

Appendix D. Supplementary data

Supplementary data to this article can be found online at https://doi.org/10.1016/j.jcis.2025.138513.

Data availability

Data will be made available on request.

References

[1] B.J. Borah, P.K. Maiti, C. Chakravarty, S. Yashonath, Transport in nanoporous zeolites: relationships between sorbate size, entropy, and diffusivity, J. Chem. Phys. 136 (2012) 174510.
[2] P. He, H. Liu, J. Zhu, Y. Li, S. Huang, P. Wang, et al., Tests of excess entropy scaling laws for diffusion of methane in silica nanopores, Chem. Phys. Lett. 535 (2012) 84–90.
[3] R. Gaur, L. Mishra, S.K.S. Gupta, Diffusion and transport of molecules in living cells, Modell. Simul. Diffusive Processes (2014) 27–49.
[4] D.J. Beltran-Villegas, T.D. Edwards, M.A. Bevan, Self-consistent colloidal energy and diffusivity landscapes in macromolecular solutions, Langmuir 29 (2013) 12337–12341.
[5] M.A. Bevan, D.C. Prieve, Hindered diffusion of colloidal particles very near to a wall: revisited, J. Chem. Phys. 113 (2000) 1228–1236.
[6] J.C. Swavola, T.D. Edwards, M.A. Bevan, Direct measurement of macromolecule-coated colloid–mucus interactions, Langmuir 31 (2015) 9076–9085.
[7] J.L. Bitter, Y. Yang, G. Duncan, H. Fairbrother, M.A. Bevan, Interfacial and confined colloidal rod diffusion, Langmuir 33 (2017) 9034–9042.
[8] A. Ledesma-Durán, L.H. Juárez-Valencia, Diffusion coefficients and MSD measurements on curved membranes and porous media, Eur. Phys. J. Eng. 46 (2023) 70.
[9] R. Kusters, C. Storm, Impact of morphology on diffusive dynamics on curved surfaces, Phys. Rev. E Stat. Nonlin. Soft Matter Phys. 89 (2014) 032723.
[10] Alipour M, Li Y, Liu H, Pahlavan AA. Diffusiophoretic transport of colloids in porous media. 2024. arXiv:2411.14712.
[11] Y. Li, J. Zou, H. Huang, J. Li, H. Zhang, J. Li, Pore structure-domoinated nonradical oxidation activity of self-dispersed Fe doped mesoporous-carbon for boosting antibiotics degradation efficiency, Sep. Purif. Technol. 362 (2025) 131742.
[12] K. Li, H. Ma, Rotation and retention dynamics of rod-shaped colloids with surface charge heterogeneity in sphere-in-cell porous media model, Langmuir 35 (2019) 5471–5483.
[13] S. Tu, X. Liu, S. Qu, Z. Yang, Unveiling colloidal transport and deposition: exploring pore network and random forest models for insights, Colloids Surf. A Physicochem. Eng. Asp. 684 (2024) 133074.
[14] O.A. Ramírez-Garza, J.M. Méndez-Alcaraz, P. González-Mozuelos, Effects of the curvature gradient on the distribution and diffusion of colloids confined to surfaces, Phys. Chem. Chem. Phys. 23 (2021) 8661–8672.
[15] A. Naji, F.L.H. Brown, Diffusion on ruffled membrane surfaces, J. Chem. Phys. 126 (2007) 235103.
[16] D. Baptista, L. Teixeira, C. van Blitterswijk, S. Giselbrecht, R. Truckenmüller, Overlooked? Underestimated? Effects of substrate curvature on cell behavior, Trends Biotechnol. 37 (2019) 838–854.
[17] W. Xi, S. Sonam, T. Beng Saw, B. Ladoux, Lim C. Teck, Emergent patterns of collective cell migration under tubular confinement, Nat. Commun. 8 (2017) 1517.
[18] Y. Zhong, L. Zhao, P. Tyrlik, G. Wang, Investigating diffusing on highly curved water-oil interface using three-dimensional single particle tracking, J. Phys. Chem. C 121 (2017) 8023–8032.
[19] C.-y. Wu, S. Tarimala, L.L. Dai, Dynamics of charged microparticles at oil−water interfaces, Langmuir 22 (2006) 2112–2116.
[20] K. Du, J.A. Liddle, A.J. Berglund, Three-dimensional real-time tracking of nanoparticles at an oil–water interface, Langmuir 28 (2012) 9181–9188.
[21] K.D. Danov, R. Dimova, B. Pouligny, Viscous drag of a solid sphere straddling a spherical or flat surface, Phys. Fluids 12 (2000) 2711–2722.
[22] I. Sriram, R. Walder, D.K. Schwartz, Stokes–Einstein and desorption-mediated diffusion of protein molecules at the oil–water interface, Soft Matter 8 (2012) 6000–6003.
[23] A.K. Pearce, T.R. Wilks, M.C. Arno, R.K. O'Reilly, Synthesis and applications of anisotropic nanoparticles with precisely defined dimensions, Nat. Rev. Chem. 5 (2021) 21–45.
[24] S. Riedel, L.A. Hoffmann, L. Giomi, D.J. Kraft, Designing highly efficient interlocking interactions in anisotropic active particles, Nat. Commun. 15 (2024) 5692.
[25] F. Hu, X. Wang, Q. Li, Characteristics and analysis of PM2.5 particles in a light-polluted atmosphere in winter, Sci. Rep. 15 (2025) 3087.
[26] V. Kudryavtseva, G.B. Sukhorukov, Features of anisotropic drug delivery systems, Adv. Mater. 36 (2024) 2307675.
[27] F. Zhou, H. Wang, Z. Zhang, Diffusion of anisotropic colloids in periodic arrays of obstacles, Langmuir 36 (2020) 11866–11872.
[28] K.V. Edmond, M.T. Elsesser, G.L. Hunter, D.J. Pine, E.R. Weeks, Decoupling of rotational and translational diffusion in supercooled colloidal fluids, Proc. Natl. Acad. Sci. 109 (2012) 17891–17896.
[29] A. Chakrabarty, A. Konya, F. Wang, J.V. Selinger, K. Sun, Q.-H. Wei, Brownian motion of boomerang colloidal particles, Phys. Rev. Lett. 111 (2013) 160603.
[30] Y. Peng, L. Lai, Y.S. Tai, K. Zhang, X. Xu, X. Cheng, Diffusion of ellipsoids in bacterial suspensions, Phys. Rev. Lett. 116 (2016) 068303.
[31] Z. Zheng, R. Ni, Y. Wang, Y. Han, Translational and rotational critical-like behaviors in the glass transition of colloidal ellipsoid monolayers, Sci. Adv. 7 (2021) eabd1958.
[32] H. Liu, Y. Zong, The curvature effect on the diffusion of single Brownian squares on a cylindrical surface in the presence of depletion attractions, Langmuir 37 (2021) 9264–9268.
[33] K. Zhao, R. Bruinsma, T.G. Mason, Entropic crystal–crystal transitions of Brownian squares, Proc. Natl. Acad. Sci. 108 (2011) 2684–2687.
[34] R.P. Mondescu, M. Muthukumar, Brownian motion and polymer statistics on certain curved manifolds, Phys. Rev. E 57 (1998) 4411–4419.
[35] P. Castro-Villarreal, Intrinsic and extrinsic measurement for Brownian motion, J. Stat. Mech.: Theor. Exp. 2014 (2014) 05017–05018.
[36] S. Paquay, R. Kusters, A method for molecular dynamics on curved surfaces, Biophys. J. 110 (2016) 1226–1233.
[37] J.E. Bond, A.J. Yeh, J.R. Edison, M.A. Bevan, Diffusion, density, and defects on spheres, Soft Matter 20 (2024) 6371–6383.
[38] H. Brenner, The slow motion of a sphere through a viscous fluid towards a plane surface, Chem. Eng. Sci. 16 (1961) 242–251.
[39] S.A. Poniaev, K.K. Soboleva, A.I. Sobolev, V.V. Dudelev, G.S. Sokolovskii, Drag coefficient of solid micro-sphere between parallel plates, J. Phys. Conf. Ser. 769 (2016) 012084.
[40] F. Manca, P.-M. Déjardin, S. Giordano, Statistical mechanics of holonomic systems as a Brownian motion on smooth manifolds, Ann. Phys. 528 (2016) 381–393.
[41] P. Castro-Villarreal, Brownian motion meets Riemann curvature, J. Stat. Mech.: Theor. Exp. 08 (2010) 08006.
[42] C. Solano-Cabrera, P. Castro-Villarreal, R. Moctezuma, F. Donado, J. Conrad, R. Castaneda-Priego, Self-assembly and transport phenomena of colloids: confinement and geometrical effects, Ann. Rev. Condens. Matter Phys. 16 (2025) 41–59.
[43] H. Goldstein, Classical Mechanics, 2nd ed, Addison-Wesley, 1980.
[44] D. Duverney, An Introduction to Hypergeometric Functions, Birkhäuser, Cham, 2024.
[45] P. Castro-Villarreal, A. Villada-Balbuena, J.M. Méndez-Alcaraz, R. Castañeda-Priego, S. Estrada-Jiménez, A Brownian dynamics algorithm for colloids in curved manifolds, J. Chem. Phys. 140 (2014) 214115.